Hearing Research, 55 (1991) 24–38

HEARES 01598

Shared-stimulus driving and connectivity in groups of neurons in the dorsal cochlear nucleus

Daryl R. Kipke [1], Ben M. Clopton [2] and David J. Anderson [2,3]

[1] *Graduate Program in Bioengineering, University of Michigan,* [2] *Kresge Hearing Research Institute, University of Michigan and* [3] *Department of Electrical Engineering and Computer Science, University of Michigan, Ann Arbor, Michigan, U.S.A.*

(Received 28 June 1990; accepted 20 February 1991)

Extracellular spike discharges were recorded from ensembles of up to five neurons simultaneously in the DCN of guinea pig using solid-state, thin-film, multichannel electrodes having up to five recording sites spanning up to 600 microns. Responses from 73 unit pairs were collected of which 54 had both units responding to pseudorandom wideband noise stimulation. Shared-stimulus driving was present in 78% (42/54) of the unit pairs and could be attributed to an overlap in their spectral sensitivities. Effective connectivity was indicated for 87% (47/54) of the unit pairs. Wideband noise proved more useful than tonebursts for investigating shared-stimulus driving and connectivity because it evoked widespread, but not overly synchronous, responses in the ensembles.

Multiunit recording; DCN; Thin-film electrode; Neural networks; Noise characterization

Introduction

Much of the work on dorsal cochlear nucleus (DCN) function has involved characterizing the responses of single units to a battery of simple sounds. This work, coupled with anatomical and morphological investigations, has revealed the complex structure and response properties of the nucleus. The guinea pig DCN, in brief, is a laminar structure consisting of a superficial molecular layer containing mostly granule cells and their parallel fibers, the fusiform cell layer containing fusiform cells oriented in a regular manner with cochlear afferents contacting their basal dendrites, and the deep layer containing giant cells (Hackney et al., 1990). There are also many smaller interneurons distributed throughout the DCN that suggest a high level of local interaction. An orderly arrangement of inputs from the auditory nerve to the fusiform and giant cells superimposes a tonotopic map on the laminar structure, approximately orthogonal to it along the mediolateral axis. Other afferents to the DCN come from the anterior ventral cochlear nucleus, inferior colliculus, and superior olivary complex. The fusiform cells and giant cells provide the major DCN outputs to the inferior colliculus. Thus, to a first approximation, a slice of the DCN along its rostrocaudal axis and through all layers would consist of principal cells which receive similarly tuned primary afferents, along with interneurons providing interactions within the slice, and across slices. This will be referred to as an 'isofrequency sheet' (Bourk et al., 1981; Ryan et al., 1988; Moore, 1986, 1989). This morphology suggests a difference in connectivity within an isofrequency sheet as compared to across sheets.

Several recurring single-unit response patterns to tonebursts have been identified and are typically classified in terms of the temporal features of the peristimulus time histogram (PSTH) taken at a single frequency-intensity combination (Pfeiffer, 1966; Bourk, 1976). In addition, classification has also been based on response rates taken over many frequency-intensity combinations, resulting in a response map (Evans and Nelson, 1973; Young and Brownell, 1976; Young and Voigt, 1982; see Young et al., 1988 for review). Single-unit discharge patterns in the DCN are typically more complex than in the ventral cochlear nucleus; most notably inhibitory areas become more prevalent. Many of the unit responses fall into three response map categories. Type II units have V-shaped response maps, little or no spontaneous activity, and no wideband noise response. Type III units have V-shaped response maps accompanied by inhibitory sidebands. Type IV units have mostly inhibitory response maps, with an excitatory region at their characteristic frequency near threshold. Several unit response types have been associated with cell types through cell staining (Rhode et al., 1983; Smith and Rhode, 1985) and antidromic stimulation (Young, 1980). Type II units are thought to correspond to intrinsic DCN interneurons, while Type IV units are thought to correspond primarily to fusiform cells.

Correspondence to: Daryl Kipke, Institute for Sensory Research, Merrill Lane, Syracuse University, Syracuse, NY 13244-5290, U.S.A. Fax: (315) 443-1184.

More complex stimuli, such as AM tones (Kim et al., 1990) and noise (Eggermont, 1983; Eggermont and Smith, 1990; Clopton and Backoff, 1991), have also been used to characterize unit responses in the DCN. Noise characterization is based on stimulating with a periodic Gaussian noise and estimating the phase coherences of the noise, referenced to frequency, that evokes spikes by the unit. The noise stimuli have been found to drive units that are tuned to frequencies over the entire noise bandwidth, and they tend to evoke less synchrony than, for example, tonebursts at CF (Backoff and Clopton, 1991).

Functional relationships between units cannot be addressed through single-unit characterizations. In this case, multiunit recordings, in which the spike activities of small groups of sparsely sampled neurons are observed separately and simultaneously, must be used. Through such studies, evidence confirms inhibitory connections, possibly monosynaptic, from Type II units to Type IV units (Voigt and Young, 1980, 1990), and of shared inputs between Type IV units (Voigt and Young, 1988). Gochin et al. (1989) did not find inhibitory relationships, irrespective of unit type, but they did find evidence of both shared inputs and unidirectional, possibly polysynaptic, connections between units. These studies employed tonal stimulation and spiketrain correlation methods. The cross-correlograms were found to be dependent on the tone frequency and level, in part because the units often had different CFs and thresholds. A given tone may drive one unit, but not the other, making it difficult to obtain crosscorrelations.

Combining noise characterization with multiunit recording and correlation analysis provides an alternative, more structured, approach for describing functional relationships between neurons. The noise provides a more efficient stimulus than tones in the sense of simultaneously driving more units tuned over a broader range of frequencies. It also evokes less synchrony, which is an important requirement for estimating stimulus effects. Finally, it allows for a useful interpretation of shared-stimulus driving between units.

Following the terminology of Gerstein et al. (1989), the term effective connectivity will be used to denote the equivalence class of neuronal circuits that can be inferred from spiketrain data. Neural synchrony will be used to denote the observed 'raw' relationships between units' spikes (Epping and Eggermont, 1987). At a first level of approximation, neural synchrony is composed of direct stimulus effects on single unit firing rates – shared-stimulus driving – and effects which arise from neural interactions between the units – effective connectivity. Shared-stimulus driving can be further decomposed into inputs from shared receptive fields and effects arising from stimulus structure. The former can be estimated with noise stimulation, while the latter is eliminated with noise stimulation. Effective connectivity can arise through relatively direct connections from one neuron to another, or through shared inputs from an unobserved neuron (or neurons) to the observed neurons; it is often difficult to discern these mechanisms from only spiketrain data.

The objective of this study was to describe shared-stimulus driving and effective connectivity in neuron pairs in the DCN under noise stimulation. Units within and across isofrequency sheets were compared. We used a newly developed solid-state multichannel microelectrode for multiunit recording, and utilized established single-unit and multiple-unit spiketrain analysis methods.

Methods

Physiological preparation

Multiunit responses were recorded from adult pigmented guinea pigs weighing 200–500 g. The animals were anesthetized with an intramuscular injection of ketamine hydrochloride (Vetalar, 100 mg/kg) and xylazine (Rompun, 5 mg/kg) and supplemented regularly to maintain appropriate levels of anesthesia. Dexamethasone (0.3 mg/kg) was sometimes given by intramuscular injection to reduce brain swelling. The animal was placed on a DC-powered heating pad, and core temperature was maintained at 37.5 °C. The skull was fixed to a rigid bar with stainless steel screws threaded into the dorsal cranium and covered with dental acrylic. The pinna and a portion of the external meatus were excised, and a Beyer DT-48 earphone in an aluminum enclosure acoustically damped with steel wool was coupled to the meatus forming a closed system. The acoustic system was calibrated for its amplitude and phase response using a B and K 0.5 inch microphone and a calibrated probe tube.

Multichannel microelectrodes (described below) and/or beveled glass micropipettes filled with 2M potassium citrate (impedance of 5–10 MΩ) were used to extracellularly record unitary spike waveforms. The posterior cranium was opened, and the cerebellum overlying the cochlear nucleus was aspirated to allow direct visual placement of the recording electrode on the surface of the DCN. The brain tissue was covered with warm 2% agar-agar in physiologic saline to prevent dessication and reduce brain pulsations. The electrode entry point, orientation and angle of entry were noted. Electrode depth from surface was monitored from the hydraulic microdrive used to advance the electrode.

Electrodes

The multichannel microelectrodes were based on solid-state, thin-film technologies (Drake et at., 1988;

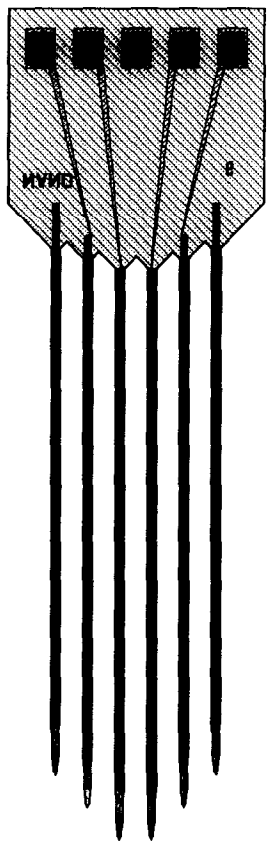

Fig. 1. The multishank solid-state electrode (NANO 6). The electrode was mounted, at its base (top), to a special printed circuit board that served as both a carrier and an interconnect to external equipment. Each shank was slightly tapered near the recording sites, located near the tip, and came to a sharp point at the tip. The shanks were just over 1.6 mm long and 30 μm wide by 12–15 μm thick at the level of the recording sites. For the electrode shown, each shank had four recording sites on one lateral surface, with each recording site having a surface area of 36 μm^2. One recording site per shank, on the four interior shanks, was connected to external equipment; the two outside shanks were not connected. The shank separation was 100 microns. A similar multishank electrode having five connected sites and a shank separation of 150 microns was also used.

BeMent et at., 1986; Najafi et al., 1985) made available by the Center of Integrated Sensors and Circuits, University of Michigan. They had five or six separate shanks 30 μm wide by 12–15 μm thick at the level of the recording sites (Fig. 1). Each shank had one or four recording sites on one lateral surface, each with a surface area of 75 μm^2 or 36 μm^2. Only four or five sites per electrode were connected to the acquisition system, with never more than one connected site per shank. The connected sites were chosen to lie along a line perpendicular to the long axis of the shanks. Electrodes had shank separations of either 100 or 150 μm, yielding an effective electrode array of equally spaced contacts spanning 400 μm or 600 μm. The recording sites of the electrodes were thin films of iridium or gold with typical impedances of 3 to 6 MΩ. Differences in site impedances for any given electrode were less than 0.5 MΩ. The electrodes used in this study were from the NANO 7 and NANO 6 electrode sets (Wise, 1989) and will be referred to here as multishank electrodes. The electrode was mounted on a special printed circuit board that served as both a carrier and an interconnect to external equipment. The bond pads on the electrode were ultrasonically bonded with aluminum wire to the circuit board and stabilized and insulated with epoxy. The circuit board was plugged into a standard integrated circuit socket that was mounted on an hydraulic micromanipulator, and connected to a set of five custom-designed amplifiers.

The multishank electrode was oriented such that the axis of the recording sites was approximately along either the mediolateral or rostrocaudal axis of the DCN, while the electrode was advanced along the dorsoventral axis. The mediolateral orientation positioned the electrode shanks across the isofrequency sheets of the DCN. The rostrocaudal orientation, normal to the mediolateral, positioned the shanks approximately within an isofrequency sheet. In one preparation both a glass micropipette and a multishank electrode were used to record units. The multishank electrode was oriented along the mediolateral axis while the pipette was positioned approximately 500 μm anterior to it.

Stimulus protocol

The stimulus set consisted of frequency-modulated (FM) tones, short duration tonebursts, and a set of synthesized periodic noise sequences. FM tones, logarithmically swept in frequency from 0.3 to 16.0 kHz (or from 16.0 to 0.3 kHz), were used as the primary search stimuli. These were digitally synthesized with an 8192-point sequence and sampled at 50 kHz resulting in a period of 163.8 ms. The tonebursts were gated analog waveforms with a duration of 40 ms. They were phase coherent across presentations, with a 5 ms rise and fall time, and were presented at a rate of 10 per second. All of the digital stimuli were synthesized off-line, stored on hard disk, and presented at 12-bit resolution through a waveform generator. Each stimulus (toneburst, FM sweep or noise sequence) was typically presented 150 or 200 times. Calibration of the acoustic system was achieved by averaging the sound pressure measured near the eardrum over several animals using tones uniformly stepped from 0.200 kHz to 20 kHz. The high frequency amplitude roll-off was compensated with an inverse filter to flatten the amplitude characteristics.

The noise stimuli consisted of 16 independent, pseudorandom noise sequences first specified in the frequency domain (the synthesis procedure was fully described in Clopton and Backoff, 1991). Each sequence was defined over a discrete spectrum of 8192 points with a frequency resolution of $\Delta f = 6.1$ Hz, i.e., $f_k =$

$k\Delta f$, where $0 \leq k \leq 8191$. This corresponds to a sampling frequency of $\Delta f(8192) = 50$ kHz and a Nyquist (aliasing) frequency of 25 kHz at $k = 4095$. Frequencies below the Nyquist frequency are positive frequencies, those above are negative frequencies. The complex Fourier coefficients in the range of 0.299 kHz to 12.207 kHz were specified to have equal, nonzero magnitudes and random phases uniformly distributed over 0 to 2π. Fourier coefficients below and above this range, up to 25 kHz, were set to zero, filling the remaining positive frequencies. The negative frequencies could then be set equal to the complex conjugates of the positive frequencies, reflected about $k = 4095$. The inverse discrete Fourier transform of the spectrum produced a real, time waveform which was quantized at a 12-bit, fixed-point amplitude resolution. The resulting waveform was presented continuously to yield a periodic stimulus (period of $T = 1/\Delta f = 163.84$ ms) with no transients at the points of repetition. The set of noise sequences approximated 16 finite-length realizations of a stationary, bandlimited Gaussian random process. Estimates of unit responses to the noise could then be improved by averaging over many periods of each sequence and also over the set of 16 sequences.

The unattenuated noises had a spectrum level of 71.2 dB RMS re 20 $\mu N/m^2$ Hz, and were usually presented at 10 to 20 dB above the threshold for driving of a unit, typically corresponding to 0 to 30 dB spectrum level. The highest spectrum level used was approximately 45 dB. Presentation of the noise set typically consisted of the first sequence being loaded into the waveform generator and presented 200 times, during which unit responses were monitored and acquired. After the end of 200 presentations, the stimulus was turned off, the spike data were saved to disk, and the second noise sequence was loaded and presented 200 times. This routine continued until the last sequence was presented or the units were lost. Gaps in stimulation between the end of the presentation of one sequence and the beginning of the next ranged from approximately 4 s to several minutes. When spontaneous rates were sufficient, the noise presentation routine was temporarily interrupted to collect spontaneous responses.

Data acquisition

The data acquisition system was an AT-class personal computer connected to a programmable timing and sampling system (Modular Instruments Inc.) controlled with software developed in our laboratory. The presentation of digital stimulus sequences, recording of spike firing times, and acoustic calibration were controlled through the system.

Spike detection was achieved with hardware window discriminators (one Frederick Haer window discriminator per data channel) adjusted to provide maximum superimposition of spike waveforms on an oscilloscope. Spike times, relative to the last stimulus onset time, were recorded with time resolution of 10 μs. During online data collection, any two of the electrode sites could be selected for unit detection, usually with one unit per site. In addition, to handle the remaining two or three electrode sites, the extracellular potentials from each electrode site, the stimulus trigger, and a voice channel were recorded using a studio quality eight-channel tape recorder (Tascam 48), thus providing a full transcript of the experiment. When the experiment was completed, unit detection was accomplished, where possible, for the electrode sites that were not selected on-line. The control information on the tape allowed for synchronization of the on-line and off-line detected unit spiketrains. The tape recorder had a maximum temporal error of 0.24% between the record and play modes. For a time interval of 20 ms, this corresponded to a maximum temporal error of 0.048 ms, which is an order of magnitude smaller than the crosscorrelogram binwidth of 0.64 ms used for analysis. The acquisition software provided displays of PSTHs and simultaneous crosscorrelograms (described below) for indicators of single unit and unit pair responses. Subsequent spiketrain analyses were done after the experiment was completed. The raw spiketrain data were stored with an information header in binary form on hard disk. The set of units simultaneously observed at a given electrode position (ranging from two to five units) was called a 'neural ensemble.'

Data analysis

Single unit and pairwise response measures were calculated for each unit pair in an ensemble to estimate stimulus coding properties of the individual units and functional relationships between the units. These measures were implemented on Unix workstations (Sun Microsystems Inc. and Apollo Computer Inc.) with a spiketrain analysis program developed in our laboratory. This program includes a database for efficient organization of the unit responses for each ensemble and a querying system that permits both interactive and batch generation of PSTHs and pairwise crosscorrelograms. Batch generated data were transferred to an Apple Macintosh II and plotted. Data management and display procedures encumbered significant resources due to the large amount of data and the number of stimulus-to-unit and unit-to-unit measures associated with each ensemble.

Crosscorrelation analysis

Standard correlation methods were used to parse the observed neural synchrony between two units into components attributable to direct stimulus effects and effective connectivity (Perkel et al., 1967; Palm et al., 1988). This procedure is formulated as an hypothesis

test in which the null hypothesis holds that all correlation is attributable to direct stimulus effects. An estimator of the correlation due to direct stimulus effects (PST predictor) is constructed and then subtracted from the raw correlation measure (simultaneous crosscorrelogram), resulting in a residual correlation measure (residual crosscorrelogram). Significant deviations of the residual crosscorrelogram from chance indicates effective connectivity between the units. This procedure assumes stationary firing rates and low levels of stimulus driving of each unit; high levels of stimulus driving are likely to cause response-rate saturation and interfere with the estimation of shared stimulus driving. It also assumes the association between the spiketrains are of first-order, and that it can be modeled as a linear combination of shared stimulus driving and effective connectivity. Through simulations, the linear combination assumption was found to be valid when the units each had a low level of stimulus driving and when they operated in the approximately linear activation range (Melssen and Epping, 1987). Noise stimulation typically provided the low level of stimulus driving required. The nominal operating region of DCN units is difficult to estimate, but was assumed to be adequate.

The simultaneous crosscorrelogram (SCC) estimates the first-order neural synchrony between spiketrains and is defined as the histogram of the forward and backward time intervals between spikes of unit A (reference unit) and all spikes by unit B (nonreference unit). The spike times of each unit, referenced to a stimulus trigger, were binned at a resolution of Δt ms and expressed as a point process $A^m(k)$, where $A^m(k) \epsilon \{0, 1\}$, $m = 0, \ldots, M-1$ indexes the stimulus presentations and $k = 0, \ldots, K-1$ is the time step index. $K = T/\Delta t$, with T defined as the stimulus period. $A^m(k)$ can be 'unfolded' with respect to stimulus triggers through the operation

$$A(k + mK) = A^m(k), \quad k = 0, \ldots, K-1;$$

$$m = 0, \ldots, M-1.$$

The SCC was calculated from the unfolded spiketrains by

$$\varphi(\tau\Delta t) = \frac{MK}{MK - \tau} \sum_{j=0}^{MK-1} A(j\Delta t)B((j+\tau)\Delta t),$$

where, τ is an integer index of time shift, $-\tau_{max} \leq \tau \leq \tau_{max}$, and Δt was chosen such that the number of spikes per bin in the original point processes did not exceed one. The term MK/MK-τ makes $\varphi(\tau\Delta t)$ an unbiased estimate with respect to edge effects. $\varphi(\tau\Delta t)$ is expressed in units of coincident spikes. Under the assumption that the units fire as independent stationary Poisson processes with average rates μ_A and μ_B, respectively, the expected number of coincident spikes in each bin of the SCC is $E[\varphi] = KM\mu_A\mu_B(\Delta t)^2$. The variance of the bin count is approximately $\sigma^2 \approx KM\mu_A\mu_B(\Delta t)^2(\mu_A\Delta t + \mu_B\Delta t + 1)$, when τ is neglibible compared to stimulus duration K (Edwards and Kipke, 1991). When the spike distribution in a bin is assumed to arise from Bernoulli trials (Pr{spike in bin τ} = p, Pr{no spike in bin τ} = 1 − p) the terms $\mu_A\Delta t$ and $\mu_B\Delta t$ are eliminated and $\sigma^2 \approx KM\mu_A\mu_B(\Delta t)^2$, which is equivalent to that commonly used (Abeles, 1982). The Bernoulli assumption begins to break down when $\mu_A\Delta t > 0.2$ or $\mu_B\Delta t > 0.2$ (Edwards and Wakefield, 1991). Assuming a Gaussian distribution of spike counts, the 95% confidence intervals can be approximated at $E[\varphi] \pm 2\sigma$. An SCC was considered significantly different than chance if two or more adjacent values lay outside the confidence intervals. This test indicates the deviation of the two spiketrains from independent stationary Poisson processes.

The next level of analysis addresses whether these deviations are a result of shared stimulus driving or effective connectivity or some combination of the two. This is achieved by estimating the component of the SCC attributable to shared stimulus driving. One method for doing this is based on circularly shifting one spiketrain an integer number of stimulus periods relative to the other spiketrain before unfolding the spiketrains and constructing a crosscorrelogram similar to that of the SCC (Perkel et al., 1967). The shifting operation serves to eliminate correlations due to effective connectivity while preserving correlations due to direct stimulus effects. The resulting shifted correlogram, the shift-predictor, has the same statistics as the SCC. The statistics can be improved if shift-predictors over many shifts are averaged.

A more desirable method of estimating direct stimulus effects is based on the cross correlation of the units' PSTHs and is called the PST predictor (Palm, 1988). If $A'(\cdot)$ and $B'(\cdot)$ are the PSTHs for units A and B, respectively, then the PST predictor is given by

$$z(\tau\Delta t) = \frac{K}{M(K-\tau)} \sum_{j=0}^{K-\tau-1} A'(j\Delta t) \times B'((j+\tau)\Delta t).$$

The expected value of $z(\tau\Delta t)$ is $E[z] = E[\varphi] = KM\mu_A\mu_B(\Delta t)^2$. The variance of the PST predictor is $\sigma^2 \approx KM\mu_A\mu_B(\Delta t)^2(\mu_A\Delta t + \mu_B\Delta t + 1/M)$ (Edwards and Kipke, 1991). The terms $\mu_A\Delta t$ and $\mu_B\Delta t$ are nonnegligible compared to $1/M$. The PST predictor represents the expected correlation of two independent, stationary, Poisson spiketrains with firing patterns exactly as that indicated by their respective PSTH.

It is equivalent to the average crosscorrelogram formed from all permutations created by 'shuffling' the stimulus periods of one spiketrain relative to the other. The circular shift operation is a restricted type of shuffling; thus, the shift-predictor can be considered a subset of the PST predictor. The shift-predictor averaged over all shifts approaches the PST predictor but is computationally prohibitive. The PST predictor provides a better estimate of shared stimulus driving with less computation.

The final step of the analysis was to calculate an estimate of the effective connectivity between units by subtracting, bin-by-bin, the shift-predictor or the PST predictor from the SCC. The result is called the residual crosscorrelogram (RCC) and is given by

$$\tau(\tau\Delta t) = \varphi(\tau\Delta t) - z(\tau\Delta t),$$

with expected value $E[\tau(\tau\Delta t)] = 0$ and variance $\sigma^2 \approx K(M-1)\mu_A\mu_B(\Delta t)^2$ (Edwards and Kipke, 1991). This procedure, in effect, normalizes the SCC with respect to direct stimulus effects so that remaining significant deviations can be attributed to effective connectivity.

In the figures, the ordinate values of the SCCs, PST predictors, and RCCs are expressed in terms of average spike rate obtained by dividing the spike count in each bin by the bin duration (Δt multiplied by the number of trigger events). The binwidth was set to 0.64 ms, and no smoothing was performed. The noise-evoked correlograms shown were the average of the correlograms constructed for each of the sixteen noise sequences. Autocorrelograms, the SCC of a unit with itself, were also calculated for each unit, and when possible, SCCs under conditions of no stimulation (spontaneous) were calculated for each unit pair. The average firing rate of each unit over the entire noise presentation interval was also monitored as an indication of stationarity.

Single-unit characterization

The primary means of single-unit characterization was the spectrotemporal receptive field (STRF) for the unit (Eggermont et al., 1983). There are two aspects to this procedure: obtaining the spectrotemporal noise representation, and obtaining an estimate of noise features which tended to evoke spikes. Complete details of this procedure are described in Clopton and Backoff (1991). Briefly, each noise was transformed using the Rihaczek distribution (Rihaczek, 1968; Cohen, 1989) to obtain a time-frequency representation of the stimulus. The time resolution was limited at 20 μs, and frequency resolution was limited at 6.1 Hz. In this study, the time resolution was usually chosen at 160 μs, and the frequency resolution at 97.7 Hz. The spectrotemporal representation for each noise stimulus was calculated at one reference frequency to obtain a 'time slice' from the time-frequency surface. That time function was then crosscorrelated with the PSTH for the unit under analysis, the PSTH being binned at the same time resolution chosen for the stimulus function. Crosscorrelation functions for corresponding frequencies were summed over the 16 noise stimuli resulting in a STRF surface. The surface was bounded by time-precedence (time relative to spike discharge) and reference frequency. These surfaces are displayed as contour plots with the minimum contour at 2 to 3 SD relative to the mean with one standard deviation steps, unless stated otherwise. Details concerning the calculation of the standard deviation are given in Clopton and Backoff (1991). Calculation of the STRFs was performed off-line.

The STRFs provided an efficient method for estimating the CFs for units in an ensemble. Previous work has shown that the reference frequency of the highest peak of an STRF obtained with noise levels 15–30 dB above threshold correlates very strongly to the CF as estimated with tonebursts (Backoff and Clopton, 1991). The CF of some units was also estimated by manually adjusting the attenuation and frequency of tonebursts while visually and acoustically monitoring spike discharge rates. The two estimates were found to be consistent.

Results

Twenty-three ensembles having a total of 65 units and 73 unit pairs were recorded from the DCN of nine guinea pigs. Four of the ensembles consisted of two units recorded with dual pipettes, 18 ensembles consisted of from two to five units recorded with multishank electrodes, and one ensemble was recorded with both a pipette (one unit) and a multishank electrode (three units). Only pairwise interactions were analyzed in the present study; ensembles with more than two units were valuable insofar as they provided an efficient means of obtaining unit pair data (an ensemble of four units provides six unit pairs; five units provides ten unit pairs). Fifty unit pairs were recorded with the multishank electrode oriented along the mediolateral axis of the DCN, and 19 pairs were recorded with the electrode oriented along the rostrocaudal axis. The positions of the pipettes relative to each other or to the multishank electrode could not be determined and are indicated as 'indeterminate' (Table I).

Responses to the noise stimuli were the basis for most single unit and pairwise analyses. Toneburst responses were obtained for some of the units in some of the ensembles but were not extensively analyzed. Each noise stimulus was presented at the same intensity level for an ensemble; this level was set such that each unit in the ensemble was driven. Eighty-five percent

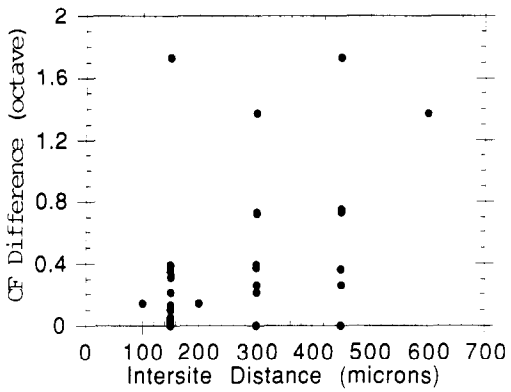

Fig. 2. Difference in CF between units, expressed in octaves, versus the separation between recording sites from which the units were recorded. Only data collected with the multishank electrode in the mediolateral orientation are shown. A direct relationship was suggested between the separation of recording sites and CF difference ($P < 0.05$).

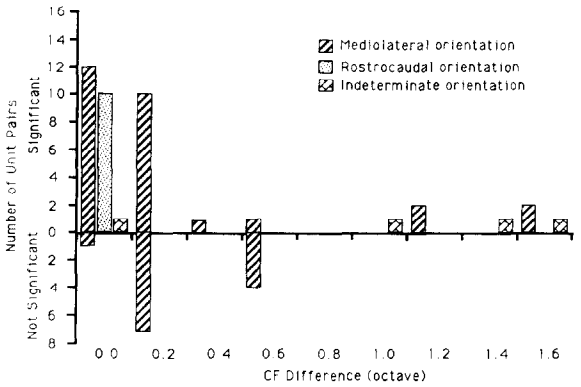

Fig. 3. Shared-stimulus driving versus CF difference. The number of unit pairs having either significant (above the abscissa) or insignificant (below the abscissa) PST predictors are shown as a function of the units' CF difference and electrode orientation. Significant PST predictors suggest shared stimulus driving between the units. Only unit pairs in which both units responded to the noise were considered, resulting in a sample of 54 unit pairs (40 pairs recorded with electrode in mediolateral orientation, 10 pairs with rostrocaudal orientation, and 4 pairs with indeterminate orientation).

(55/65) of the units responded to the noise in a significant manner as indicated by STRFs having at least one region with multiple matrix values lying more than 2.5 SD from the mean stimulus surface. Both units responded to the noise in 74% (54/73) of the unit pairs; most of the subsequent analysis will be done on this data set. The reference frequency of the maximum value of the STRF for each unit was used to estimate CF (Backoff and Clopton, 1991). Within an ensemble, the STRFs of the units responding to the noise were generally unique based on indicators such as spectral extent of significant features, CF, shape of significant features and precedence times to significant features. A relationship was suggested ($P < 0.05$) between recording site separation and CF difference, expressed in octaves, for unit pairs observed with a multishank electrode oriented along the mediolateral axis of the DCN (Fig. 2). All unit pairs recorded along the rostrocaudal orientation had CFs within 0.2 octaves.

The incidence of shared-stimulus driving versus difference in CF was evaluated for unit pairs in which both units responded to noise. The PST predictor was used to estimate shared-stimulus driving. CF differences ranged from 0 to approximately 1.6 octaves, with 87% (47/54) of the unit pairs having a difference below 0.8 octaves (Fig. 3). Seventy-eight percent (42/54) of the unit pairs exhibited a significant PST predictor. The incidence of shared-stimulus driving was not found to be related to either CF difference or electrode orientation, but it was associated with an overlap in the spectral extent of the units' STRFs. A large variability in spectral extent was observed such that the STRFs of two units with relatively close CFs, but spectrally narrow STRFs, may not overlap in frequency, while those of units with a larger CF difference and broader STRFs may overlap. The PST predictor features were often quite sharp temporally (widths ranging from 1–4 ms) and were either symmetrical about the zero-delay point, or offset less than 10 ms. Many PST predictors exhibited more than one significant feature and could often be explained through similarities in STRFs.

An analysis of the incidence of effective connectivity versus difference in CF, using the same set of unit pairs in which both units responded to noise, found that 87% (47/54) of the pairs exhibited a significant RCC, taken to indicate an effective connection be-

TABLE I

DATA SUMMARY

Electrode Orientation	No. of Ensembles	No. of Units	No. of Unit Pairs	Noise Characterized	
				No. of Units	No. of Unit Pairs
Mediolateral	12	38	50	34	40
Rostrocaudal	7	19	19	13	10
Indeterminate	4	8	4	8	4
Totals	23	65	73	55	54

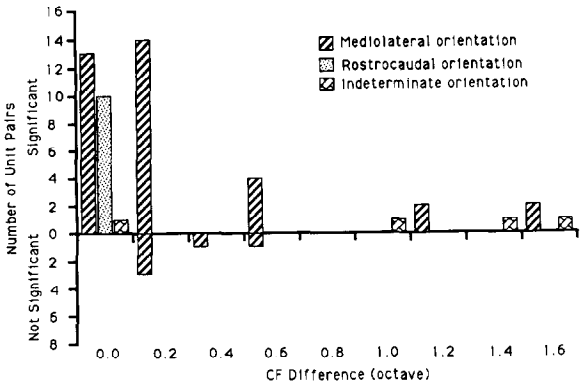

Fig. 4. Effective connectivity versus CF difference. Using the same data set as in Fig. 3, the number of unit pairs having either significant (above the abscissa) or insignificant (below the abscissa) residual crosscorrelograms (RCCs) are shown as a function of the units' CF difference and electrode orientation. Significant RCCs suggest an effective connection between the units.

tween the units (Fig. 4). Again, no relationships were found between the incidence of effective connectivity and CF difference, or between effective connectivity and electrode orientation. In all unit pairs that exhibited a significant RCC, the primary feature was a sharp peak, either symmetric about the zero-delay point or offset less than 5 ms. The former would suggest shared input from an unobserved neural source while the latter suggests a short-delay excitatory effective connection. RCC features, typically less than 2 ms wide, were, in general, narrower than the peaks in the PST predictor for the same unit pair.

The STRFs for a typical ensemble (D35:3) are shown in Fig. 5. This ensemble was composed of four units recorded with a multishank electrode oriented along the mediolateral axis of the DCN, approximately 500 microns from the surface. The noise set evoked highly significant STRFs from units 1, 3, and 4, but only a minimal response from unit 2. The STRFs of units 3 and 4 contained troughs (striped contours), but at a smaller significance level than the peaks. While the general shape of the primary features in the STRFs from units 1, 3, and 4 were similar, the spectral extent and precedence time of each differed. In many ensembles, the STRF feature shapes themselves were also different. The SCC, PST predictor, and RCC for three of the six unit pairs of this ensemble are shown in Fig. 6. These three unit pairs were selected to illustrate the span of features often seen within an ensemble. The SCC for unit pair 1|2 (i.e., the discharge rate of unit 1 given unit 2 has fired at the origin) exhibited a sharp symmetric peak centered around zero delay preceded by a broader less significant knee extending from -1 to -3 ms relative to unit 2 spikes. The PST predictor for this unit pair was statistically flat resulting in an RCC essentially equivalent to the SCC (Fig. 6A). This suggests an effective connection between units 1 and 2 that evoked both a highly significant number of near-coincidence spikes, and a smaller number of spikes by unit 1 one to three ms before unit 2. The lack of shared-stimulus driving is consistent with unit 1's highly significant STRF and unit 2's marginal STRF–unit 2 was not driven by the noise but unit 1 was; they had no shared stimulus input. Unit pair 3|4 exhibited a combination of shared-stimulus driving and effective connectivity (Fig. 6B). The sharp peak near zero-delay in the SCC could be largely attributed to effective connectivity, while the smaller, wider peak at approximately -3 ms could be attributed to shared-stimulus driving. This feature was consistent with the units' STRFs, which contained peaks separated by 2.5 to 3 ms, with unit 3 leading unit 4. A similar analysis of the crosscorrelograms for unit pair 1|4 suggests that these units were related mostly through shared-stimulus driving (Fig. 6C). The delay to the peak of the PST predictor again

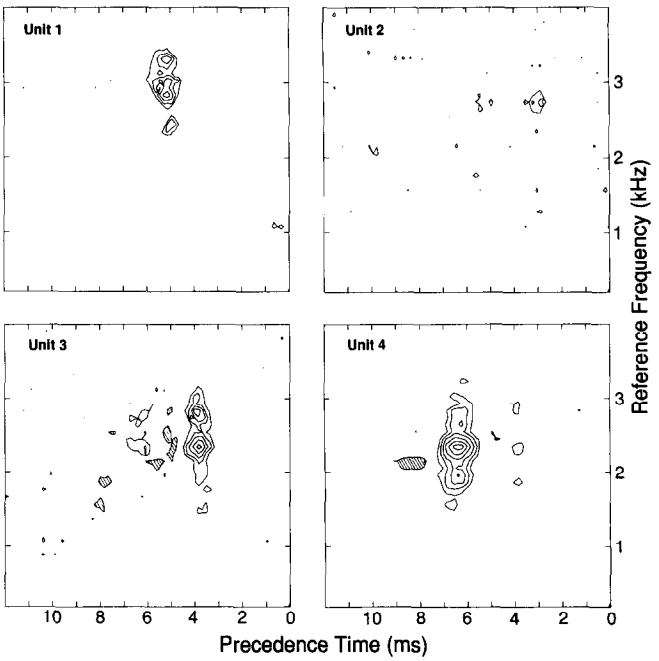

Fig. 5. Contour plots of the spectrotemporal receptive fields (STRFs) for each of the four units in ensemble D35:3. In this and other STRFs, the resolution is 160 microseconds by 97.7 Hz; positive deviations from the mean stimulus energy surface (peaks) are shown as open contours, negative deviations (troughs) as a single striped contour. Spike discharge occurred at zero precedence time. The CF of the unit is estimated by the reference frequency of the highest peak in the STRF. The STRFs were calculated from the responses to all 16 of the noise stimuli, unless noted otherwise. Unit 1: minimum contours set to ± 3.0 standard deviations (SDs) with 1.0 SD steps (ΔSD). Maximum peak of 6.8 SDs, relative to the mean level, was located at a reference frequency of 2.93 kHz and precedence time of 5.12 ms. The STRF was based on $N = 2747$ spikes. Unit 2: minimum contour at ± 2.5 SD; ΔSD = 1.0; peak of 3.87 SD at 2.84 kHz and 3.36 ms; $N = 2015$ spikes. Unit 3: minimum contour at ± 2.5 SD; ΔSD = 1.5; peak of 9.22 SD at 2.45 kHz and 4.0 ms; $N = 2806$ spikes. Unit 4: minimum contours at ± 2.5 SD; ΔSD = 2.0; peak of 13.68 SD at 2.45 kHz and 6.56 ms; $N = 8733$ spikes.

was consistent with the differences in precedence times to the peaks in the units' respective STRFs.

An analysis of STRFs, autocorrelograms, and crosscorrelograms could provide a means of describing circuits of an ensemble's functional structure. An ensemble (D22:5) consisting of four units recorded with a multishank electrode oriented along the rostrocaudal axis of the DCN will be used as an example. The STRFs of this ensemble indicated that the units all had CFs in the range of 3 kHz, and that each unit responded strongly to the noise set (Fig. 7). The autocorrelograms of each unit exhibited primary features consistent with the temporal patterning observed in its STRF (Fig. 8). The STRFs for units 1 and 4 contained multiple bands at precedence times of approximately 2.5 ms for unit 1, and 2.5, 4, and 7 ms for unit 4. These delays were similar to the delays between features in the respective autocorrelograms. Units 2 and 3 exhibited a single band in their STRFs and correspondingly very little patterning in their autocorrelograms. The autocorrelogram of some units, e.g., unit 4 of this ensemble, contained secondary, often oscillatory, features that suggest more complex processes than implied at the present level of analysis; an extensive treatment of these data is beyond the scope of this paper (see Kim et al., 1990).

The SCCs, PST predictors, and RCCs for unit pairs 1|3 and 1|4 are shown in Fig. 9. The features in the PST predictors corresponded to those expected from a comparision of the respective STRFs indicating a type of shared receptive field between the units, i.e., similar stimulus features tended to evoke responses by the units. The RCC for unit pair 1|3 is suggestive of an effective connection from unit 3 to unit 1, with a delay of approximately 4 ms that could arise from either a shared neural input, with a differential delay of 4 ms, to the units, and/or from a polysynaptic neural connection from unit 3 to unit 1, with a cumulative delay of 4 ms. The RCC for unit pair 1|4 indicated near-coincidence firing symmetrically distributed about zero-delay. This type of effective connectivity could arise from a shared input to the units having similar delays.

Some of the units exhibited onset responses to the noise that violated the stationarity assumptions assumed for correlation analysis. The onset responses were typically characterized by a brief initial period after a noise sequence was turned on, over which the unit had a relatively high firing rate, followed by an approximately exponential decrease of firing rate to a steady state value over the remainder of the noise stimulus presentation time (Clopton and Backoff, 1991).

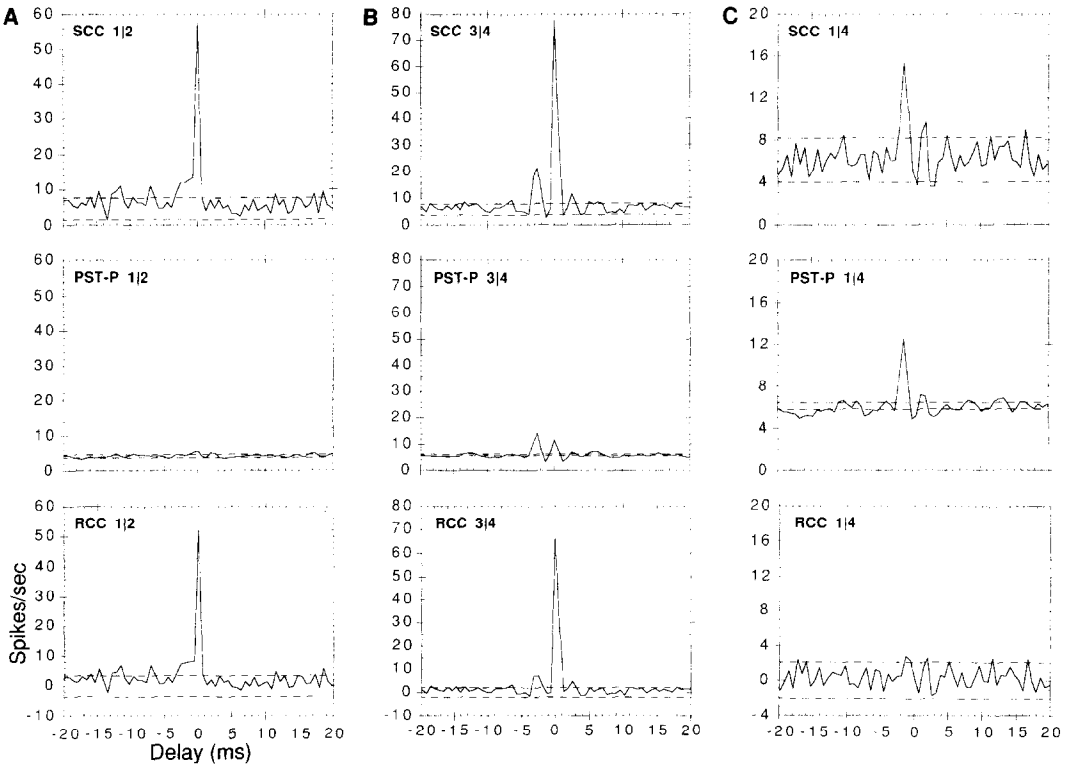

Fig. 6. The set of crosscorrelograms for three of the six unit pairs from ensemble D35:3. The SCC (top), PST predictor (middle), and RCC (bottom) for a unit pair are arranged in a single column. See the text for explanation of each of these measures. Unit pair 1|2 indicates the crosscorrelogram for unit 1 given unit 2. For ease of comparision, the ordinates are constant for each unit pair; the abscissas are all the same. The binwidth was 0.64 ms. Each measure was calculated over all 16 noise stimuli, unless noted otherwise. The approximate 95% confidence intervals are shown as dotted lines. See description of Fig. 5 for number of spikes from each unit.

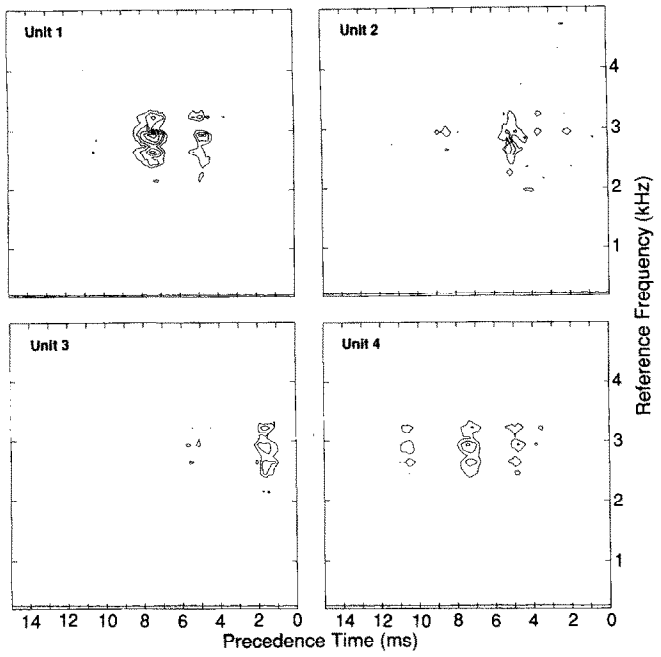

Fig. 7. STRFs of the four units of ensemble D22:5. See Fig. 5 for STRF display details. These units responded to noise features over the same frequency range, but with different precendence times and temporal patterns. The minimum contours were 2.0 SD for each unit. Unit 1: peak of 7.05 SD at 2.83 kHz and 7.52 ms; $N = 4166$ spikes. Unit 2: peak of 3.5 SD at 2.83 kHz and 5.44 ms; $N = 2308$ spikes. Unit 3: peak of 3.94 SD at 3.12 kHz and 1.76 ms; $N = 3043$ spikes. Unit 4: peak of 4.16 SD at 2.83 kHz and 7.68 ms; $N = 8913$ spikes.

The average firing rates of two simultaneously recorded units (D35:2, units 1 and 5) that exhibited this onset response to each of fifteen noise sequences are shown in Fig. 10 (data from the sixteenth sequence were not

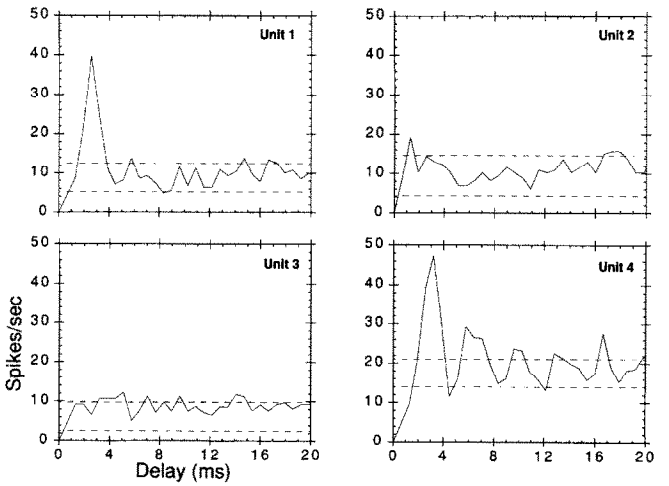

Fig. 8. Autocorrelograms for the four units of ensemble D22:5. Display details are given in Fig. 6, unit summaries in Fig. 7. Only short-term (< 20 ms) properties of the unit's firing were considered. The primary features (or lack thereof) of the unit's autocorrelogram were generally consistent with the pattern of peaks in its STRF.

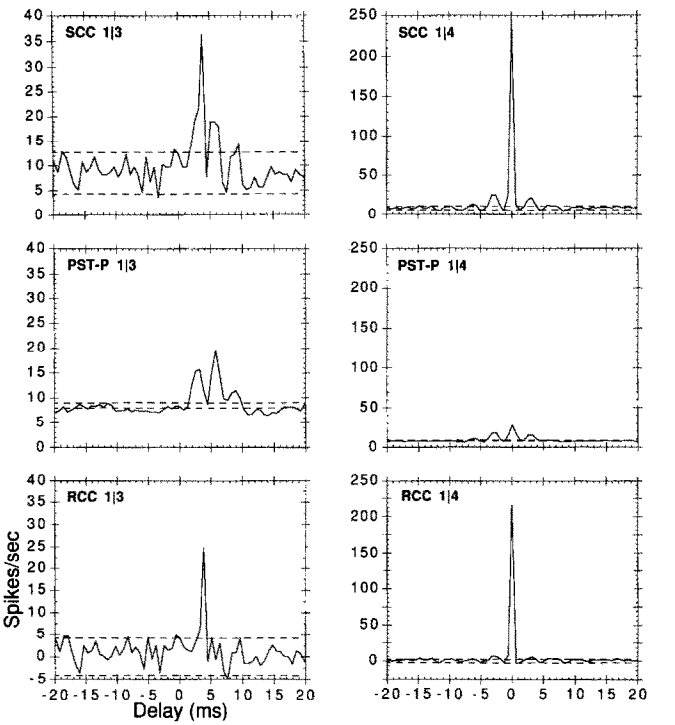

Fig. 9. The set of crosscorrelograms for unit pairs 1|3 and 1|4 of ensemble D22:5. Display details are given in Fig. 6, unit summaries in Fig. 7. The PST predictor for each of these unit pairs is consistent with features in the units' STRFs.

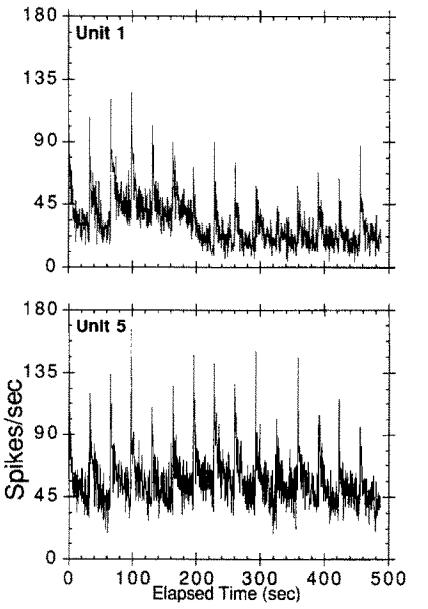

Fig. 10. Average firing rates, over fifteen noise stimuli, of units 1 and 5 of ensemble D35:2. Each noise was presented continuously for 32.8 s (200 periods). Here, the presentation intervals for all of the noises were concatenated, without gaps, resulting in a cumulative elapsed presentation time of 491 s. Spikes were counted over bins of 0.5 s and were plotted as average rate over each bin (spike resolution was 10 μs). Both of these units displayed a characteristic onset response when each noise was turned on that decayed to a steady-state level after approximately 6–10 s.

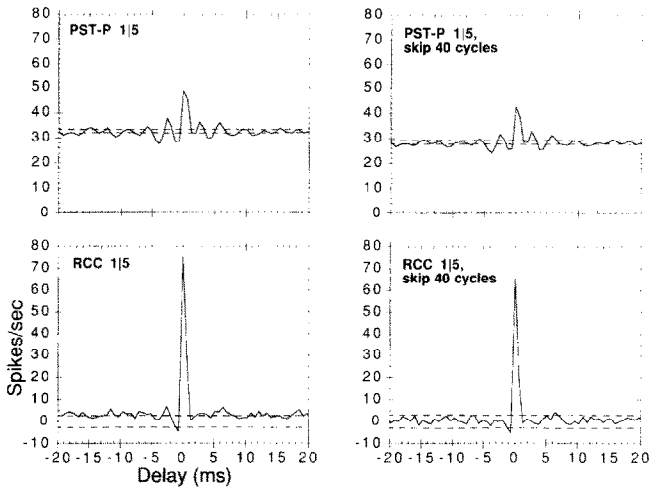

Fig. 11. PST predictors and RCCs for unit pair 1|5 of ensemble D35:2. Shown in the left column are the PST predictor and RCC calculated using the complete cumulative noise presentation time, i.e., the entire duration of each of the fifteen noise stimuli used for this ensemble. Shown in the right column are the PST predictor and RCC calculated using a partial noise presentation time, in which the first 40 periods of each noise stimulus were omitted; this corresponded to the first 6.6 s of each noise presentation. This interval contains the high onset response of each unit. The features of the PST predictor and RCC did not change when the onset spikes were omitted.

available). Each sequence had a period of 163.8 ms and was presented 200 times resulting in a total presentation time of 32.8 s. In the figure, the presentation times of the fifteen noises were concatenated without gaps; during the experiment, the presentation of each noise sequence was followed by intervals of approximately 4 s to several minutes during which no sound was presented. The steady state firing rates of each unit were essentially constant over all the noises, with the exception of unit 1 over noise stimuli 3 through 6. The PST predictor and RCC for this unit pair calculated over the complete noise presentation interval are shown in Fig. 11. The same measures calculated over the interval in which the first 40 periods of each noise were skipped (6.4 s; 20% of the presentations) are also shown. The primary features of the PST predictor and RCC did not change when the onset times were omitted, though the absolute rates did decrease because of fewer spikes. For this 20% decrease in the number of stimulus presentations, the number of spikes by unit 1

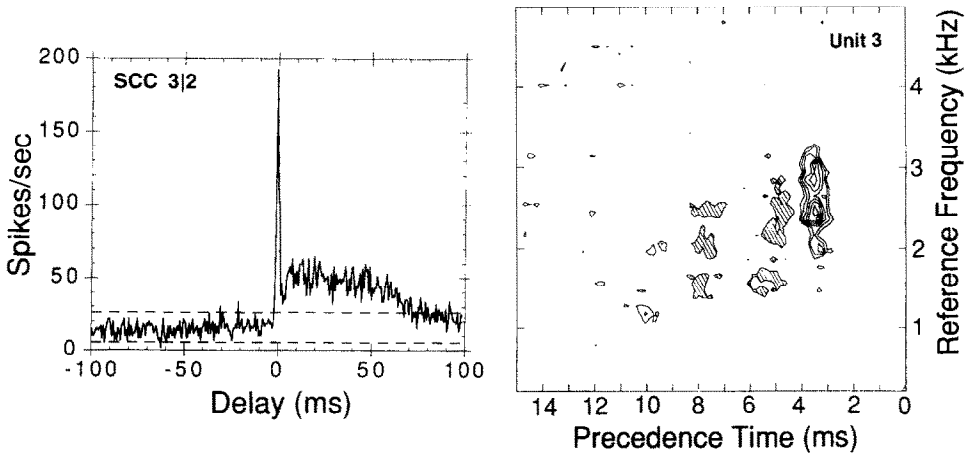

Fig. 12. Long-term interaction between units in ensemble D35:4. Left: SCC for unit pair 3|2 over a maximum delay of ±100 ms. This is characterized by a high number of near-coincident spikes, and an elevated conditional firing rate of unit 3 that lasted approximately 70 ms. The PST predictor for this unit pair was not significant. Right: The STRF of unit 3. The minimum positive contour was 2.5 SD, with ΔSD = 1.0; the minimum negative contour was 2.2 SD. Peak of 7.95 SD at 2.54 kHz and and 3.68 ms. Unit 2 did not respond to the noise. Based on 963 and 8463 spikes for units 2 and 3, respectively.

decreased by 30% (16032 spikes to 11170 spikes), while the number of spikes by unit 5 decreased 28% (28002 spikes to 20235 spikes).

One unit pair (D35:4, units 2 and 3) exhibited a long-term interaction lasting approximately 75 ms. This pair was recorded using a multishank electrode oriented along the mediolateral axis of the DCN approximately 500 μm from the surface. Both units responded strongly to tonebursts around 2 kHz, with unit 2 having a higher threshold than unit 3. Unit 3 was noise driven with a STRF having a highly significant peak over the frequency range of 2–3 kHz followed by less significant troughs (Fig. 12). Unit 2 was not driven by the noise and did not exhibit a significant STRF. The average firing rates were 1.8 spikes/s for unit 2 and 16.2 spikes/s for unit 3. The SCC for unit pair 3|2 indicated a pronounced asymmetric correlation extending to approximately 75 ms relative to unit 2 spike times (Fig. 12). The PST predictor was statistically flat; thus, the significant SCC features could be attributed to effective connectivity between the units. The features consisted of a sharp, highly significant correlation symmetric about zero-delay, followed by a later, lower significance long-duration correlation. Thus, unit 2 tended to fire when unit 1 fired, and then also underwent an extended period of elevated firing rate.

Discussion

In interpreting these results we assume the PST predictor and RCC to be indicators of shared-stimulus driving and effective connectivity, respectively. For these observations of 54 relatively closely spaced, noise-driven, unit pairs in the DCN, effective connectivity was indicated in 87% of the pairs. Shared-stimulus driving was slightly less common, present in 78% of the pairs encountered. Many unit pairs exhibited both shared stimulus driving and effective connectivity. Shared stimulus driving was associated with an overlap in the frequency-response range as determined by the units' STRFs. For pairs with shared stimulus driving, the peak structure of the PST predictor could usually be associated with the peak structures of the STRFs allowing for appropriate delays. Associating troughs in the PST predictors with minor STRF troughs was sometimes possible but less certain, in part because these features were not common. This suggests that the fine temporal features in PST predictors due to shared stimulus driving were imposed by the relative afferent delays associated with each unit in a pair. Significant features in the RCCs were typically sharp, highly significant peaks either symmetrically positioned about the zero delay point, or offset less than 5 ms. Inhibitory features, points significantly less than the average RCC level, were rarely observed.

We did not observe significant differences in the incidence and features of either shared stimulus driving, or effective connectivity, as a function of electrode orientation. This was somewhat unexpected because of the distinctly different morphology of the DCN along its mediolateral and rostrocaudal axes. Because of the limited sample population and uncertainty about precise electrode positions, these data should be considered as preliminary.

From the properties of the noise stimuli and the manner in which the PST predictor was calculated as an average over all of the noise sequences, shared stimulus driving indicated that the units tended to fire in response to similar specific features of the noise. One physiological interpretation is that the units received inputs from an overlapping set of primary afferents, each with an associated delay, that evoked precise rate modulation. The noise stimuli tended to evoke temporally sharp peaks in PSTHs, as compared to tonebursts. This can help explain why significant features in the PST predictor were often narrower than the symmetric 'central mound' that was observed under tonal stimulation (Voigt and Young, 1988).

Both the unit-to-unit and stimulus-to-unit characterization methods adopted in this work are based on correlation analysis. The former provides a basis for parsing nonchance correlations into components suggestive of shared-stimulus driving and effective connectivity, an analysis which has a long history of study and discussion (Perkel et al., 1967; Gerstein and Perkel, 1972). The latter constructs a structured complex stimulus environment within which spike discharges are associated with immediately preceding time patterns of phase coherence in a wideband Gaussian noise. This STRF approach has been developed more recently (Eggermont et al., 1983; Eggermont and Smith, 1990) and was found to be a replicable estimator of tuning and delay in the mammalian CN (Clopton and Backoff, 1991; Backoff and Clopton, 1991). We have found this complex stimulus environment to be very useful for investigating functional relationships between units and for providing an interpretation of shared stimulus driving. The percentage of units we found to be driven by the noise was lower, but generally comparable to that reported previously. Relationships between STRF patterning, PST predictors, and autocorrelograms are not yet been fully understood, but can conceivably arise from, in part, shared afferent inputs, afferent pathways with different delays and inherent membrane properties of the neuron (Backoff and Clopton, 1991).

The thin-film, multichannel electrodes were a very important tool in this investigation. The fixed geometry and replicable electrical characteristics of the recording sites made the electrodes well suited for sampling neural populations in a regular, systematic manner. The electrodes were fabricated in batches containing

several hundred electrodes each, resulting in similar electrode types having similar electrical characteristics. Important properties of the electrodes were their durability, flexibility, and strength, which are all derived from the silicon substrate (Najafi et al., 1990; Najafi and Hetke, 1990). The electrodes can be custom designed for a given series of experiments in order to exploit properties of the neural structure under study. In this study, the multiple shank design made consistent sampling within, and across, isofrequency sheets a relatively simple process. A complementary study could utilize electrodes with a single shank and linearly arranged sites to sample units in a single isofrequency layer from superficial to deep layers.

The observations of the present study are generally consistent with previous work in identifying characteristics of effective connectivity in the DCN, but it is difficult to compare the results directly because of dissimilar experimental procedures. Specifically, noise stimulation can be expected to evoke different functional relationships, as compared to the tonal stimulation of previous work, as evidenced by crosscorrelograms that are sensitive to stimulus context (Voigt and Young, 1988). In addition, the stimulus type can cause a bias in the types of units recorded, e.g., Type II units do not respond to wideband noise (by definition), thus we would not expect such units in our sample population. In contrast to Voigt and Young's work (1980, 1990), we did not observe inhibitory relationships consistent with a monosynaptic inhibitory connection between Type II units and Type IV units (i.e., between interneurons and principal cells). Finally, because of electrode geometry and recording site characteristics, the multishank electrode used in this study may preferentially record different types of neurons as compared to pipettes. Based on previous results (Backoff and Clopton, 1991), we hypothesize that most of the units we recorded were Type IV units, i.e., fusiform or giant cells (Rhode et al., 1983).

In spite of these differences, certain general results can be compared across the studies. In the present study, both shared inputs and excitatory, unidirectional, effective connections were found to be prevalent and widely distributed in the DCN. Gochin, et al. (1989) found very similar relationships using toneburst stimulation and crosscorrelation analysis techniques comparable to ours. Voigt and Young (1988) found a high incidence of shared inputs between Type IV-Type IV units having similar CFs under both spontaneous and stimulated (long-duration tones) conditions. These previous studies used either a single electrode, or dual, independently advanced electrodes, and toneburst (Gochin et al.), or long duration tone (Voigt and Young) stimulation paradigms. These experimental methods have evolved from the long history of single unit studies, but it is as yet unclear if they are sufficient for elucidating inherently more complex multiple unit relationships.

Our approach to the characterization problem for multiunit activity, and the one traditionally adopted, assumes no a priori model of the CN; it is largely descriptive. It does, however, focus analysis on pairwise comparisons. While this theoretically does not limit the number of units that can be studied simultaneously, practical considerations do. For N simultaneous spiketrains, $(N^2-N)/2$ comparisions are necessary. Our largest ensemble of five units required only 10 comparisions, but the combinatorical increase in pairwise associations is restrictive when going to, say, 10 units which allow 45 pairwise comparisions or 15 units which allow 105 comparisions. The difficulty of interpreting the network implications of such large numbers of comparisions limits the analysis. Gerstein and Aertsen (1985) have developed an analysis and visualization technique, based on a gravitational clustering algorithm, useful for identifying firing synchrony within large ensembles of 10–30 neurons. This approach does not inherently address function, underlying anatomical structure, or stimulus coding, but it does provide a workable method of identifying subgroups of units that merit further analysis. As electrode and acquisition system technologies continue to advance, it will become more practical to record the spike activities of larger groups of units and the limiting factor in multiunit investigations will be data analysis methods. Model-based system identification methods may provide a solution (e.g., Brillinger, 1988 and Chornoboy, et al., 1988). With this general approach, the pairwise comparision problem is eliminated, response dynamics can be addressed, and quantitative predictions of ensemble responses can be made, but limitations arise through the inherent difficulty in mathematically describing realistic functional relationships, especially in CNS structures.

As multiunit data from the auditory system have become increasingly available, the difficulties preventing a unique determination of underlying structure from multiple spiketrain data have become more apparent. Major reasons for the difficulties are: limitations of correlation methods, lack of quantification of stimulus effects, limitations of spike data, and undersampling of the neural population. Crosscorrelation analysis, as applied in this study, is a time average. Insofar as the physiological processes and stimulus influences involved are not stationary, the crosscorrelograms and STRFs will not be representative of the full data segment. In particular, short-term dynamic changes in connectivity and rapid changes in the effectiveness of different stimulus attributes will be obscured. While some response parameters were monitored, such as triggering on the spike waveform, average rate, and overall stimulus driving, no extensive analyses were made to detect less obvious nonstation-

arities. Furthermore, no analyses or corrections were made for the effects of spike-discharge history such as refractoriness (Johnson and Swami, 1983; Bi, 1989), although this was not likely to be a significant influence due to the relatively low average spike rates for all of the units observed. Techniques for detecting dynamic changes in connectivity and stimulus driving have been proposed (Aertsen et al., 1989; Schneider et al., 1983), but were not implemented in this study. Understanding how units share and transmit stimulus information is an important aspect of describing neural function, but one which has not been adequately addressed in the past.

The data reported here suggest that multiunit spike data cannot distinguish discharge patterns that are due to circuitry from those due to intrinsic properties of the observed neurons unless the observed ensemble exhausts the possible members of a circuit. For example, the STRFs for units 3 and 4 in Fig. 5 have trough areas which imply that decrements in energy, in addition to the increments indicated by STRF peaks, tend to precede spike occurrence for these units. This is suggestive of inhibition or spike suppression and might arise from either circuitry or intrinsic membrane properties of the neuron (Backoff and Clopton, 1991). Either intracellular recording or an exhaustive identification of possible circuitry might resolve these alternatives. However, the latter depends on a 'proof by exception,' direct observation of inhibitory interneurons which might mediate this relationship between the stimulus and spike discharge. None of the results in this study support such a mechanism, but this cannot be taken as strong evidence against it because of the problem of undersampling.

Undersampling of the neural population, as suggested above, imposes a severe limit on the ability to describe, or functionally identify a neural structure. In general, even after the other major problems are adequately addressed, the observed units account for only a small fraction of the activity of the structure, and are not sufficient for identifying the functional system. Additional information, such as anatomical properties, types of neurons recorded, stimulus knowledge, etc. is needed to constrain the analysis. This ancillary information is becoming available for the DCN and work towards incorporating it into the analysis procedure is proceeding.

Summary and Conclusions

Pseudorandom Gaussian noise stimuli provided a structured stimulus set that was useful for investigating shared stimulus driving and effective connectivities between relatively closely spaced unit pairs in the DCN. Fifty-four unit pairs were recorded that were noise driven, both within and across isofrequency sheets. Unit separation ranged from approximately 100 to 600 μm.

Shared stimulus driving, estimated from the PST predictor, was associated with an overlap in the spectral extents of the units' STRFs. It was not related to electrode orientation. Temporal patterning of the PST predictor was often consistent with temporal features between the STRFs, leading to an interpretation of shared receptive fields.

Effective connectivity was not related to either electrode orientation or the difference in characteristic frequencies of the units. Excitatory connectivities attributable to both shared inputs and neural, possibly polysynaptic, connections were observed. This was found to be generally consistent with previous results.

Inhibitory effective connectivity between units was not observed, contrary to previous results. The type of unit involved in the inhibitory relationship, Type II units, may not have been observed in the present study because they generally show little, if any, noise response.

Acknowledgements

We thank James Wiler and Dr. Patricia Backoff for their contributions in the laboratory and, with the addition of Brent Edwards, for their comments on this manuscript. We thank Jamille Hetke for her assistance with electrode fabrication. This work was supported by grants NS 05785 from the NIH and BNS-8609850 from the NSF.

References

Abeles, M. (1982) Quantification, smoothing, and confidence limits for single-units' histograms. J. Neurosci. Methods 5, 317–325.

Aertsen, A.M.H.J., Gerstein, G.L., Habib, H.K. and Palm, G. (1989) Dynamics of neuronal firing correlation: modulation of 'effective connectivity'. J. Neurophysiol. 61, 900–917.

Backoff, P.M. and Clopton, B.M. (1991) A spectrotemporal analysis of DCN single unit responses to wideband noise in guinea pig. Hear. Res. 53, 28–40.

BeMent, S., Wise, K.D., Anderson, D.J., Najafi, K., and Drake, K.L. (1986) Solid-state electrodes for multichannel multiplexed intracortical neuronal recording. IEEE Trans. Biomed. Eng. BME-33, 230–241.

Bi, Q. (1989) A closed-form solution for removing the dead time effects from the poststimulus time histograms. J. Acoust. Soc. Am. 85, 2504–2513.

Bourk, T.R., Mielcarz, J.P. and Norris, B.E. (1981) Tonotopic organization of the anteroventral cochlear nucleus of the cat. Hear. Res. 4, 215–242.

Bourk, T.R. (1976), Electrical responses of neural units in the anteroventral cochlear nucleus of the cat. Doctoral dissertation, Mass. Inst. Technology, Cambridge, MA.

Brillinger, D. (1988) Maximum likelihood analysis of spike trains of interacting nerve cells. Biol. Cybern. 59, 189–200.

Chornoboy, E.S., Schramm, L.P. and Karr, A.F. (1988) Maximum likelihood identification of neural point process systems. Biol. Cybern. 59, 265–275.

Clopton, B.M. and Backoff, P.M. (1991) Spectrotemporal receptive fields of neurons in cochlear nucleus of guinea pig. Hear. Res. 52, 329–344.

Cohen, L. (1989) Time-frequency distributions - A review. Proc. IEEE, 77, 941–981.

Drake, K.L., Wise, K.D., Farraye, J., Anderson, D.J. and Bement, S.L. (1988) Performance of planar multisite microprobes in recording extracellular single-unit intracortical activity. IEEE Trans. Biomed. Eng. BME-35. 719–732.

Edwards, B. and Wakefield, G.H. (1990) On the statistics of binned neural point processes: the Bernoulli approximation and AR representation of the PST histogram. Biol. Cybern. 64, 145–153.

Edwards, B. and Kipke, D.R. (1991) Confidence intervals for period histograms, crosscorrelograms, and PST predictors under stationary and nonstationary conditions. (in preparation).

Eggermont, J.J. and Smith, G.M. (1990) Characterizing auditory neurons using the Wigner and Rihacek distributions: A comparision. J. Acoust. Soc. Am. 87, 246–259.

Eggermont, J.J., Johannesma, P.I.M. and Aertsen, A.M.H.J. (1983) Reverse-correlation methods in auditory research. Quart. Rev. Biophysics, 16, 341–414.

Epping, W.J.M. and Eggermont, J.J. (1987) Coherent neural activity in the auditory midbrain of the grassfrog. J. Neurophysiol. 57. 1464–1483.

Evans, E.F., Nelson, P.G. (1973) The responses of single neurones in the cochlear nucleus of the cat as a function of their location and the anesthetic state. Exptl. Brain Res. 17, 428–442.

Gerstein, G.L. and Aertsen, A.M.H.J. (1985) Representation of cooperative firing activity among simultaneously recorded neurons. J. Neurophysiol. 54, 1513–1528.

Gerstein, G.L. and Perkel, D.H. (1972) Mutual temporal relationships among neuronal spike trains. Biophys. J. 12, 453–473.

Gerstein, G.L., Bedenbaugh, P. and Aertsen, A. (1989) Neuronal assemblies. IEEE Trans. Biomed. Eng. BME-36, 4–14.

Gochin, P.M., Kaltenbach, J.A. and Gerstein, G.L. (1989) Coordinated activity of neuron pairs in anesthetized rat dorsal cochlear nucleus. Brain Res. 497, 1–11.

Hackney, C.M., Osen, K.K. and Kolston, J. (1990) Anatomy of the cochlear nucleus complex of guinea pig. Anat. Embryol. 182, 123–149.

Johnson, D.H. and Swami, A. (1983) The transmission of signals by auditory-nerve fiber discharge patterns. J. Acoust. Soc. Am. 74, 493–501.

Kim, D.O., Sirianni, J.G. and Chang, S.O. (1990) Responses of DCN-PVCN neurons and auditory nerve fibers in unanesthetized decerebrate cats to AM and pure tones: Analysis with autocorrelation/power spectrum. Hear. Res., 45, 95–113.

Melssen, W.J. and Epping, W.J.M. (1987) Detection and estimation of neural connectivity based on crosscorrelation analysis. Biol. Cybern. 57, 403–414.

Moore, J.K. (1989) Dorsal cochlear nucleus: cortical organization as revealed by the Golgi technique and anterograde transport of horseradish peroxidase. J. Comp. Neurol. (submitted).

Moore, J.K. (1986) Cochlear nuclei: relationship to the auditory nerve. In: R.A. Altschuler, R.P. Bobbin, and D.W. Hoffman (Eds.), Neurobiology of Hearing: The Cochlea, Raven Press, New York. pp. 283–302.

Najafi, K., Ji, J. and Wise, K.D. (1990) Scaling limitations of silicon multichannel recording probes. IEEE Trans Biomed. Eng. BME-37, 1–11.

Najafi, K. and Hetke, J. (1990) Strength characterization of silicon microprobes in neurophysiological tissues. IEEE Trans Biomed. Eng. (in press).

Najafi, K., Wise, K.D. and Mochizuki, T. (1985) A high-yield IC-compatible multichannel recording array. IEEE Trans. Elect. Dev. ED-32, 1206–1211.

Palm, G., Aertsen, A.M.H.J. and Gerstein, G.L. (1988) On the significance of correlations among neuronal spike trains. Biol. Cyber. 59, 1–11.

Perkel, D.H., Gerstein, G.L. and Moore, G.P. (1967) Neuronal spike trains and stochastic point processes II. Simultaneous spike trains. Biophysical J. 7, 419–440.

Pfeiffer, R.R. (1966) Classification of response patterns of spike discharges for units in the cochlear nucleus: tone-burst stimulation. Exp. Brain Res. 1, 220–235.

Rhode, W.S., Oertel, D. and Smith, P.H. (1983) Physiological response properties of cells labeled intracellularly with horseradish peroxidase in cat dorsal cochlear nucleus. J. Comp. Neurol. 213, 426–447.

Rihaczek, A.W. (1968) Signal energy distribution in time and frequency. IEEE Trans. Inf. Th. IT-14, 369–374.

Ryan, A.F., Furlow, Z., Woolf, N.K. and Keithley, E.M. (1988) The spatial representation of frequency in the rat dorsal cochlear nucleus and inferior colliculus. Hear. Res. 36, 181–190.

Schneider, J., Eckhorn, R. and Reitbock, H. (1983) Evaluation of neuronal coupling dynamics. Biol. Cybern. 46, 129–134.

Smith, P.H. and Rhode, W.S. (1985) Electron microscopic features of physiologically characterized, HRP-labeled fusiform cells in the cat dorsal cochlear nucleus. J. Comp. Neurol. 237, 127–143.

Voigt, H.F. and Young, E.D. (1990) Cross-correlation analysis of inhibitory interactions in Dorsal Cochlear Nucleus. J. Neurophysiol. 64, 1590–1610.

Voigt, H.F. and Young, E.D. (1988) Neural correlations in the dorsal cochlear nucleus: pairs of units with similar response properties. J. Neurophysiol. 59, 1014–1032.

Voigt, H.F. and Young, E.D. (1980) Evidence of inhibitory interactions between neurons in dorsal cochlear nucleus. J. Neurophysiol. 44, 76–96.

Wise, K.D. (1990) Passive Multichannel Recording and Stimulating Arrays Catalog, Center of Integrated Sensors and Circuits, University of Michigan, June, 1990.

Young, E.D., Shofner, W.P., White, J.A., Robert, J-M. and Voigt, H.F. (1988) Response properties of cochlear nucleus neurons in relationship to physiological mechanism. In: G.M. Edelman, W.E. Gall and W.M. Cowan (Eds.), Auditory Function, John Wiley and Sons, New York.

Young, E.D. (1984) Response characteristics of neurons of the cochlear nuclei. In: C I Berlin (Ed.), Hearing Science, College-Hill Press, San Diego.

Young, E.D. and Voigt, H.F. (1982) Response properties of Type II and Type III units in dorsal cochlear nucleus. Hear. Res. 6, 153–169.

Young, E. D. (1980) Identification of response properties of ascending axons from dorsal cochlear nucleus. Brain Res. 200, 23–37.

Young, E.D. and Brownell, W.E. (1976) Responses to tones and noises of single cells in dorsal cochlear nucleus of unanesthetized cats. J. Neurophysiol. 39, 282–300.